Int. J. Electrochem. Sci., 14 **(2019)** 6123 – 6132, doi: 10.20964/2019.07.68

International Journal of
ELECTROCHEMICAL
SCIENCE
www.electrochemsci.org

Phosphorous Modified Metal Boride as High Efficiency HER Electrocatalyst

Yiteng Liu, Jian Zhang, Xianxian Li, Zhaowei Zeng, Xu Cheng, Yadong Wang[*]*, and Mu Pan*

State Key Laboratory of Advanced Technology for Materials Synthesis and Processing, Wuhan University of Technology, Wuhan 430070, China
[*]E-mail: ywang@whut.edu.cn

Received: 9 March 2019 / *Accepted:* 10 May 2019 / *Published:* 10 June 2019

The investigation on highly active and durable electrocatalysts for the hydrogen evolution reaction (HER) is of great significant for renewable energy technologies. Herein, we report the fabrication of a series of amorphous Co_{10-x}-Ni_x-B-P nanocomposites via a facile chemical reduction and phosphorization method. Compared to the Ni-B-P, Co-B-P, and other Co_{10-x}-Ni_x-B-P electrodes, the $Co_{8.5}$-$Ni_{1.5}$-B-P nanocomposite catalyst exhibited the highest HER electrocatalytic activity in alkaline solution. The overpotential of $Co_{8.5}$-$Ni_{1.5}$-B-P is 145 mV at a current density of 10 mA cm^{-2}, and a low Tafel slope of 60.5 mV dec^{-1} is realized. $Co_{8.5}$-$Ni_{1.5}$-B-P also exhibits superior durability, showing no obvious degradation after 50 hours. These new phosphorous-modified borides are proved to be a new low-cost and high-efficiency catalyst system for water splitting.
.

Keywords: Boride, hydrogen evolution reaction, phosphide, HER catalyst, water splitting

1. INTRODUCTION

Much effort has been put into searching for sustainable energy resources because of increasing environmental concerns and decreasing non-renewable energy sources. Hydrogen is regarded as the most promising energy resource, and it has the advantages of creating zero pollution and having an excellent energy storage density [1,2]. Water splitting is one of the most outstanding methods for producing hydrogen [3]. Water splitting involves the hydrogen evolution reaction (HER) and oxygen evolution reaction (OER), both of which require high overpotential to realize the related reactions [4]. To improve the water splitting efficiency, catalysts that have high HER and OER activity must be used during the electrolysis process to accelerate the sluggish kinetics of the reaction. Precious metals such

as Pt show favorable properties for water splitting electrocatalysis. However, the high-price and the low-earth-abundance of Pt limited its wide application and commercialization [5,6]. Therefore, high activity electrocatalysts that are low cost and high earth-abundant have become the preferred target of researchers [7,8].

Recently, transition metal elements (Fe, Co, Ni, Mo, and W) composited with non-metal elements (S, Se, B, C, N, and P) have been widely used in electrolytic HER. Transition metal phosphides (TMPs) and transition metal borides (TMBs) are the typical representatives in HER and OER because of their low-price, high-earth-abundance, and outstanding activity, such as NiP [9], CoP [10], MoP [11], FeP [12], CoB [13], NiB [14], and NiFeB [15].

TMPs are interstitial compounds that have a significant amount of surface active sites and thus have excellent catalytic activity. *Zhuang* [16] prepared N, P-doped graphene cobalt Co_2P as a HER electrocatalyst, and the activity was comparable to that of Pt-group electrocatalysts. P can scramble electrons from metal atoms because of its strong electronegativity, and it can also act as a Lewis base when it comes into contact with positively charged protons during the HER process. *Popczun* [17] synthesized Ni_2P nanocomposites via a solvothermal method using tri-n-octylphosphine (TOP) as the phosphorus source, and the nanocomposites exhibited high HER catalytic activity. Compared with single-metal phosphides, the addition of a second metal can further enhance the electrocatalytic performance through the synergistic effect of the metals. Thus, much effort had been devoted to investigating bimetallic phosphides. *Du* [18] synthesized 3D nest-like NiCoP using a hydrothermal method, and NiCoP showed much higher electrochemical activity than single metal phosphides of CoP and NiP.

Boride can also serve as a precursor that can be phosphorized via phosphate reduction to synthesize transition metal phosphorus boride. The introduction of boron can improve the electrical conductivity of materials and can further boost the electrochemical performances. Both Co-and Ni-based catalysts show superior catalytic activity, especially when they are in the form of borides because B can protect Co and Ni from being oxidized. B is preferentially oxidized over Ni and Co, and thus, Ni and Co as catalyst active center of HER can be saved [19]. Adding P to a transition metal also greatly improves the HER performance of the material [20]. Together, P and B synergistically enhance a metal's catalytic HER performance. Transition metal borides have been widely reported as eletrocatalysts, although phosphorous borides have rarely been reported.

There are many ways to synthesize TMPs, including solvothermal methods [21], organometallic decomposition [22], electrodeposition [23], nanophosphate precursor synthesis [24], metal organic precursor decomposition [17], and phosphate reduction [25]. Among these methods, phosphate reduction is a simple and safe way to synthesize TMPs.

In this work, we synthesized a series of Co_{10-x}-Ni_x-B-P nanocomposite catalysts via an ordinary chemical reduction and phosphorization and investigated their HER electrocatalytic properties. Compared to other Co_{10-x}-Ni_x-B-P catalysts used for HER in 1M KOH electrolyte, the $Co_{8.5}$-$Ni_{1.5}$-B-P electrocatalyst exhibited the best electrocatalytic properties. Fairly low overpotentials of 145 mV and 162 mV at current density of 10 mA cm^{-2} and 20 mA cm^{-2} for HER are realized, respectively.

2. MATERIALS AND METHODS

2.1. Chemicals and Materials

Cobalt chloride hexahydrate ($CoCl_2·6H_2O$), nickel chloride hexahydrate ($NiCl_2·6H_2O$), sodium hydroxide (NaOH), sodium borohydride ($NaBH_4$), and sodium hypophosphite ($NaH_2PO_2·H_2O$) were purchased from Aladdin. Ethanol was purchased from Sinopharm Chemical Reagent Co., Ltd. All of the reagents were analytical grade and were used directly in the experiments without any further treatments.

2.2. Preparation of Co_{10-x}-Ni_x-B-P

Co_{10-x}-Ni_x-B-P was prepared via ordinary chemical reduction and phosphorization, as shown in Fig.1. In this chemical formula, x represents the molar content of $NiCl_2·6H_2O$ and has values from 0.5 to 2. First, 10 mmol of $CoCl_2·6H_2O$ and $NiCl_2·6H_2O$ were dissolved in 100 mL of deionized water. NaOH (0.1 M) and $NaBH_4$ (0.3 M) were mixed in 50 mL of deionized water. Using a syringe, NaOH and $NaBH_4$ solutions were then slowly added into the mixture under stirring. Once the production of bubbles was no longer observed, the black products were washed and filtered with deionized water and ethanol to remove the ionic impurities. Last, the filtered powder was dried at 60˚C for 24 h in a vacuum drying chamber to obtained dried Co_{10-x}-Ni_x-B.

Co_{10-x}-Ni_x-B and $NaH_2PO_2·H_2O$ (metal: P = 1:5) were placed in different porcelain boats with $NaH_2PO_2·H_2O$ at the intake port of a tube furnace. Finally, the samples were heated at 300℃ for 2 h under a N_2 atmosphere.

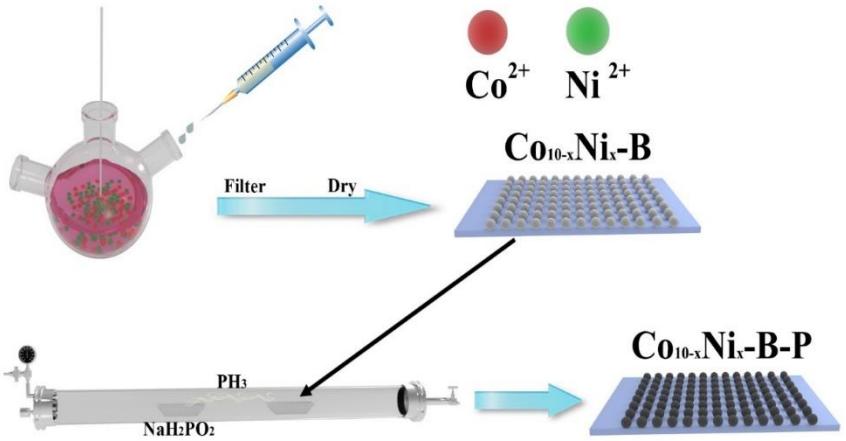

Figure 1. The preparation process of Co_{10-x}-Ni_x-B-P catalyst.

2.3. Structural Characterizations.

X-ray power diffraction patterns were recorded using an Empyrean diffractometer. Transmission electron microscopy (TEM) and scanning electron microscopy (SEM) were conducted

on a TEM JEM 2100F and FE-SEM Zeiss Ultra Plus to characterize the structure and size distribution of the synthesized nanoparticles. X-ray photoelectron spectroscopy (XPS) was recorded on an ESCALAB 250 Xi X-ray spectrometer.

2.4. Preparation of Catalyst Modified Glassy Carbon (GC) Electrode.

Catalyst inks were composed of 5 mg of catalyst powder, 970 μL of isopropanol, and 30 μL of 5% Nafion. The mixture was exposed to ultrasonic radiation for 45 min. Catalyst ink (8 μL) was loaded on the surface of the GC electrode (diameter of 0.3 cm) and then dried naturally for at least half an hour.

2.5. Electrochemical Measurements.

All of the electrochemical activities tests for HER were conducted on a CHI660E electrochemical workstation using a three-electrode configuration at 25 ℃. The electrolyte was 1 M KOH solution (pH=14), Ag/AgCl was used as the reference electrode, a graphite rod was used as the counter electrode, and the catalyst-modified GC electrode served as the working electrode. All of the measured potentials were converted to RHE (Reversible Hydrogen Electrode) using the equation: E (RHE) = E (Ag/AgCl) + 0.197 + 0.059 pH. The obtained HER polarization curves are all presented using the iR-compensation calculated according to the following equation: $E_{corr} = E_{mea} – iR$. E_{corr} is the iR-compensated potential, E_{mea} is the measured potential, and R is the ohmic resistance.

3. RESULT AND DISCUSSION

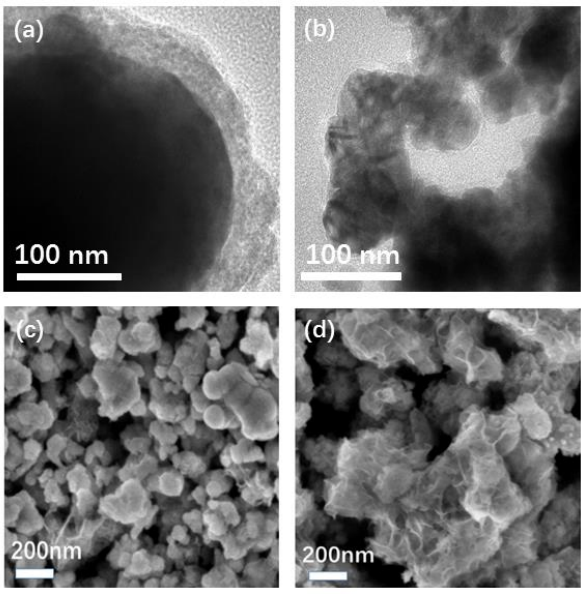

Figure 2. TEM images of $Co_{8.5}$-$Ni_{1.5}$-B (a) and $Co_{8.5}$-$Ni_{1.5}$-B-P (b); SEM images of Co8.5-Ni1.5-B (c) and Co8.5-Ni1.5-B-P (d)

TEM and SEM were used to characterize the size distributions and the morphologies of $Co_{8.5}$-$Ni_{1.5}$-B and $Co_{8.5}$-$Ni_{1.5}$-B-P, and the results are presented in Fig. 2. The $Co_{8.5}$-$Ni_{1.5}$-B-P nanoparticles had a uniform size distribution with diameters of about 60-80 nm and mainly 70 nm. By comparison, $Co_{8.5}$-$Ni_{1.5}$-B had a diameter size of more than 200 nm. The HR-TEM image inset in Fig. 3 (a) Shows no apparent crystalline phase and the selected area electrodiffraction (SAED) pattern indicates that there are diffused rings, which demonstrates that $Co_{8.5}$-$Ni_{1.5}$-B-P is amorphous. Compared to the relatively smooth particle surface of $Co_{8.5}$-$Ni_{1.5}$-B, the phosphated $Co_{8.5}$-$Ni_{1.5}$-B-P had a sheet-like morphology, which would favor a large amount of electroactive catalytic centers.

The XRD patterns (Fig. 3(b)) of the $Co_{8.5}$-$Ni_{1.5}$-B and $Co_{8.5}$-$Ni_{1.5}$-B-P nanocomposites catalyst powders showed a single broad peak centered around $2\theta = 45°$. This indicates that the nanocomposite catalyst powders that were produced via chemical reduction and solid-state phosphorization had a strong amorphous nature [2], and this is consistent with the HR-TEM results. However, after phosphorization, the $Co_{8.5}$-$Ni_{1.5}$-B-P nanocomposite catalyst powders exhibited a fairly sharp diffraction peak at an angle of $2\theta = 41°$. According to the CoNiP standard spectrum (PDF# 71-2336), the peak of $2\theta = 41°$ could be attributed to the P that results from the phosphorization.

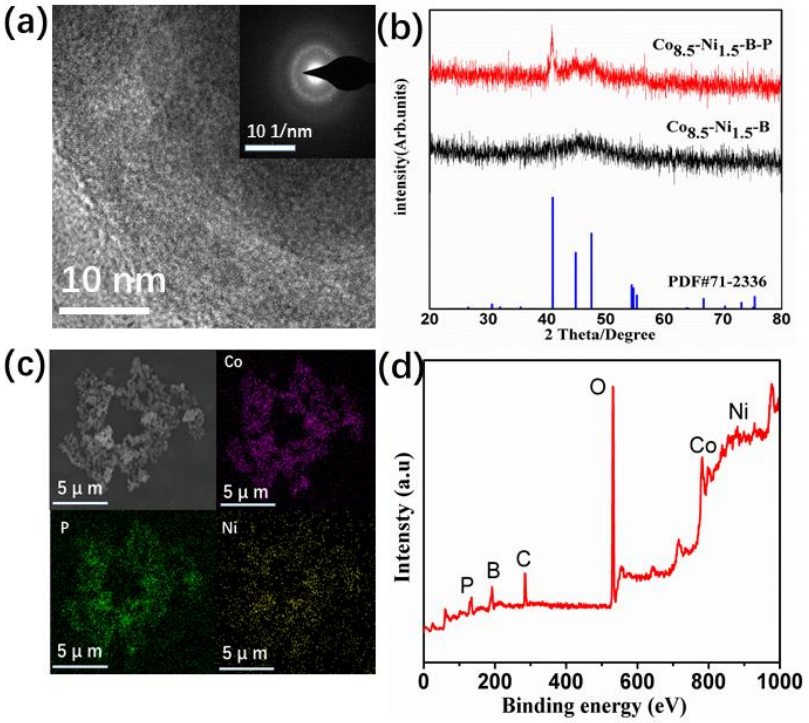

Figure 3. (a) The HR-TEM image and SAED pattern (inset) of $Co_{8.5}$-$Ni_{1.5}$-B-P catalyst; (b) The XRD pattern of the $Co_{8.5}$-$Ni_{1.5}$-B and $Co_{8.5}$-$Ni_{1.5}$-B-P catalyst; (c) The EDS elemental mapping of Co, Ni, B and P; (d) The XPS survey spectrum for $Co_{8.5}$-$Ni_{1.5}$-B-P catalyst.

Energy dispersive X-ray spectrometry (EDS) analysis of the $Co_{8.5}$-$Ni_{1.5}$-B-P nanocomposite catalysts are shown in Fig. 3(c). The EDS results indicate that the composition elements were evenly distributed in the as-prepared particles. Only Ni, Co, and P were found, but boron was not because the molecular weight was too low to be detected.

The elemental composition and valence distribution of the constituent elements of the $Co_{8.5}$-$Ni_{1.5}$-B-P nanocomposite catalysts were analyzed using XPS. The XPS survey spectrum of the $Co_{8.5}$-$Ni_{1.5}$-B-P nanocomposite catalysts reveals the presence of the elements Ni, Co, B, and P (Fig. 3 d). The signals for O and C are attributed to surface oxidation or surface adsorption of the $Co_{8.5}$-$Ni_{1.5}$-B-P nanocomposite catalysts that result from exposure to air [26]. Fig. 4(a) shows the high-resolution XPS spectrum of Ni 2p. The fitted peak at 853.4 eV corresponds to Ni in zero valence state bonded to B. The fitted peaks at 856.7 eV and 862.0 eV are attributed to the presence of NiO and $Ni(OH)_2$ [27]. Apart from these three fitted peaks, another three fitted peaks are observed at 872.6 eV, 875.1.0 eV, 881.8 eV, which are assigned to the split peak of $Ni(OH)_2$ and NiO, the energy loss peak, and the vibration peak of the Ni electron, respectively [28]. In the high-resolution Co 2p XPS spectrum (Fig. 4(b), the fitting peak at 798.0 eV belongs to Co $2p_{1/2}$. The fitting peaks at 778.9 eV and 782.0 eV correspond to Co $2p_{3/2.}$ The other fitting peaks at 787.3 eV and 803.3 eV are attributed to vibration peaks [29]. For the B 1s high-resolution XPS spectrum (Fig. 4(c), the fitting peaks of B 1s are 187.5 eV and 192.2 eV, which belong to elemental boron and boron oxide. The peaks that correspond to B were positively shifted compared to the peaks that correspond to pure boron (187.1 eV) [30]. This indicates that B provides some electrons to the Ni or Co alloys. In the P 2p high-resolution XPS spectrum (Fig. 4(c), the fitted peaks at 129.1 eV and 130.0 eV belong to P $2p_{3/2}$ and P $2p_{1/2}$, and the other fitted peak at 133.4 eV is attributed to an oxidation peak that corresponds to the P-O of the $Co_{8.5}$-$Ni_{1.5}$-B-P nanocomposite catalysts [26].

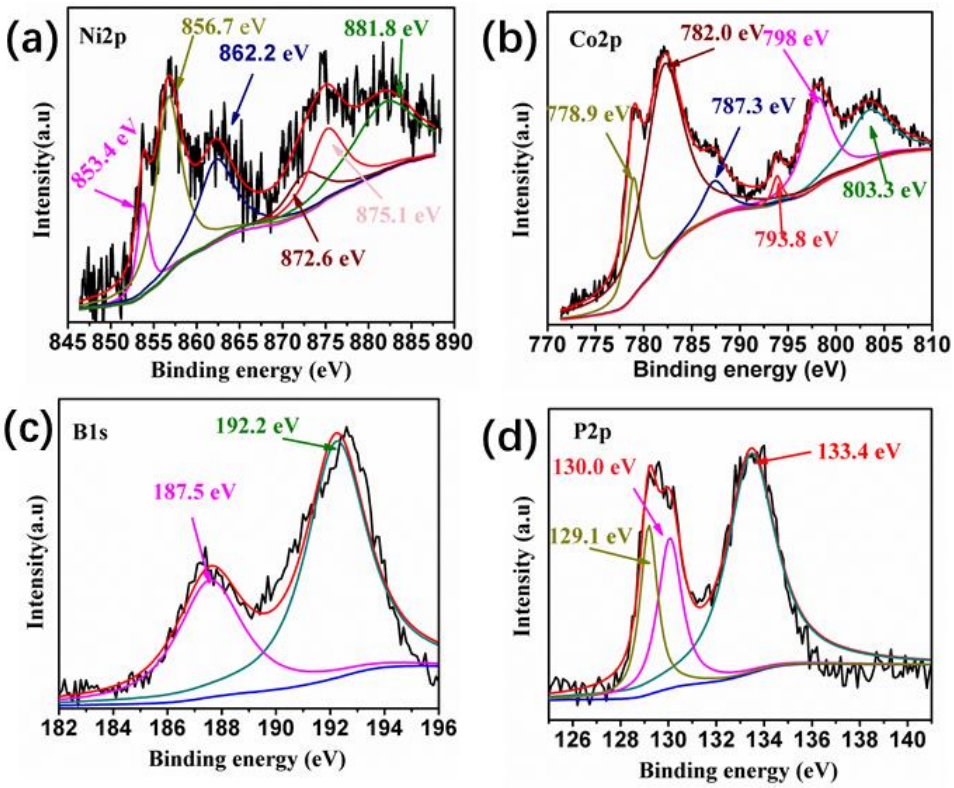

Figure 4. The high-resolution XPS spectra of (a) Ni 2p; (b) Co 2p; (c) B 1s; (d) P 2p for $Co_{8.5}$-$Ni_{1.5}$-B-P nanocomposites catalysts

The synthesized catalyst was loaded onto a GC electrode to assess the electrochemical properties. All of the electrochemical tests were performed in 1.0 M KOH at a scan rate of 5 mV s^{-1} in a three-electrode system. IR compensation was applied to eliminate the effect of Ohmic resistance to assess the intrinsic catalytic activity of catalysts. The mass loading for all the catalysts was 0.564 mg cm^{-2}. Fig. 5(a) shows the polarization curves of Ni-B, Ni-B-P, Co-B, and Co-B-P. With P doping, both the Ni-B-P and Co-B-P electrodes showed lower overpotential (η) for HER than Ni-B and Co-B. To achieve a current density of 10 mA cm^{-2}, the overpotential of Ni-B-P was 47.99 mV which is lower than that of Ni-B, and for Co-B-P, it was 30.33 mV which is lower than that of Co-B. Lower overpotential means high HER efficiency and thus high catalytic activity of electrocatalyst. These lowered overpotential values suggest that the phosphorous modification enhanced the catalytic activity of single metal boride for HER. This enhancement was more obvious for bimetallic compounds, as seen in Fig. 5(b). The $Co_{8.5}$-$Ni_{1.5}$-B-P electrode required overpotential of merely 145 mV at a current density of 10 mA cm^{-2}, which is 213 mV lower than the required overpotential for $Co_{8.5}$-$Ni_{1.5}$-B. The lower overpotential for phosphorus boride catalysts implies that they have superior HER activity and efficiency. This overpotential is also lower than that of many other reported similar HER catalysts in alkaline solution, including Ni_3S_2/NF[31], Ni_2P [32], Ni_5P_4 films [33], Co_9S_8-NixSy/Ni foam [34], CoP/CC [35], NiCoS [36], and NiCoP [37].

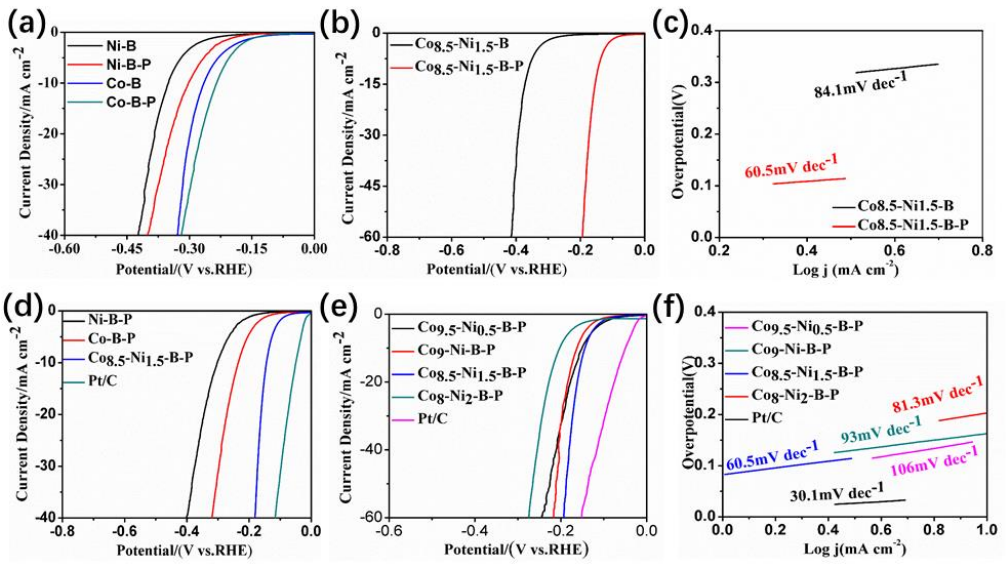

Figure 5. (a) Linear polarization curves of Ni-B, Ni-B-P, Co-B and Co-B-P catalysts; Linear polarization curves (b) and corresponding Tafel curves (c) of $Co_{8.5}$-$Ni_{1.5}$-B and $Co_{8.5}$-$Ni_{1.5}$-B-P catalysts; (d) Linear polarization curves of Ni-B-P, Co-B-P, $Co_{8.5}$-$Ni_{1.5}$-B-P and Pt/C; Linear polarization curves (e) and corresponding Tafel curves (f) of Pt/C and Co_{10-x}-Ni_x-B-P nanocomposites catalysts with different x (x is the Ni content, i.e., 0.5/9.5, 1/9, 1.5/8.5, and 2/8);

The detail overpotential comparison of different catalysts can be found in Table 1. It is obvious that the presence of P is very beneficial for lowering the overpotential. To further probe the electrochemical properties of HER, the Tafel curves of $Co_{8.5}$-$Ni_{1.5}$-B and $Co_{8.5}$-$Ni_{1.5}$-B-P are presented in Fig. 5(c). $Co_{8.5}$-$Ni_{1.5}$-B-P has a Tafel slope value of 60.5 mV dec^{-1} which is lower than that of $Co_{8.5}$-

$Ni_{1.5}$-B. The observed Tafel slope values indicate that the rate-determining step is the Volmer reaction and that HER occurs on $Co_{8.5}$-$Ni_{1.5}$-B-P via a Volmer-Heyrovsky mechanism [38]. Ordinarily, a lower slope value indicates that the catalyst (in this case, $Co_{8.5}$-$Ni_{1.5}$-B-P) has higher inherent electrochemical activity. The Tafel slope values decreased after boride phosphorization, and this also shows that the synergy of P and B greatly accelerates the electron transfer rate and improves the HER performance of the catalyst.

Table 1. Comparison of HER performance for Co8.5-Ni1.5-B-P with other HER electrocatalysts in alkaline solution.

Catalyst	η_{10}(mV)	Ref.
Ni_3S_2/NF	223	31
Ni_2P	230	32
Ni_5P_4 films	155	33
Co_9S_8-NixSy/Ni foam	163	34
CoP/CC	209	35
NiCoS	280	36
NiCoP	150	37
$Co_{8.5}$-$Ni_{1.5}$-B-P	145	This work

The polarization curves of $Co_{8.5}$-$Ni_{1.5}$-B-P in Fig. 5 (d) exhibiting higher HER catalytic activity than Ni-B-P, Co-B-P, demonstrate superior performance of bimetallic phosphorus borides. To investigate the effects of the transition metal content on electrochemical performance, phosphorus borides with different Co/Ni ratios were synthesized and tested. The polarization curves of Co_{10-x}-Ni_x-B-P nanocomposite catalysts with different values of x (where x is the Ni content, i.e., 0.5/9.5, 1/9, 1.5/8.5, and 2/8) are shown in Fig. 5 (e). Clearly, the commercial Pt/C has the highest HER catalytic activity. The $Co_{9.5}$-$Ni_{0.5}$-B-P, Co_9-Ni-B-P, $Co_{8.5}$-$Ni_{1.5}$-B-P, and Co_8-Ni_2-B-P electrodes merely overpotentials of merely 150.98 mV, 163.08 mV, 145 mV, and 203 mV, respectively, at a current density of 10 mA cm^{-2}. Thus, to obtain a current density of 20 mA cm^{-2}, the overpotentials were 178.04 mV, 184.18 mV, 162 mV, and 228.63 mV. Therefore, $Co_{8.5}$-$Ni_{1.5}$-B-P exhibited the best HER performance at both the current density values of 10 mA cm^{-2} and 20 mA cm^{-2}. These results demonstrate that proper Ni-doping improves HER activity of phosphorus borides. To clearly understand the reason for the HER performances observed with different metal ratios, the Tafel curves of catalyst materials with different metal ratios were obtained (Fig. 5(f)). The Tafel slope of Pt/C was 30.1 mV dec^{-1}, which suggests that Pt/C has excellent catalytic performance. The Tafel slope of $Co_{8.5}$-$Ni_{1.5}$-B-P (60.5 mV dec^{-1}) was lower than those of $Co_{9.5}$-$Ni_{0.5}$-B-P (106 mV dec^{-1}), Co_9-Ni-B-P (93 mV dec^{-1}), and Co_8-Ni_2-B-P (81.3 mV dec^{-1}), and this indicates that $Co_{8.5}$-$Ni_{1.5}$-B-P had much better inherent electrocatalytic activity.

The stability of a catalyst is a greatly significant parameter for the application of a catalyst. Thus, the stability of the $Co_{8.5}$-$Ni_{1.5}$-B-P catalyst material at constant current electrolysis was tested. The chronopotentiometry test was performed at a current density of 10 mA cm^{-2} in 1 M KOH. As seen in Fig. 6, the overpotential output changed only slightly from the initial overpotential for the electrode

after 50 h, and this indicates the good stability of this catalyst in alkaline solutions. During the chronopotentiometry test, the result curve shows many undulations and wrinkles because the electrodes produced a large number of hydrogen bubbles during the test, and these hindered the electron transfer and cause attenuation in the catalytic performance. When the bubbles were discharged, the catalyst exhibited the original catalytic activity.

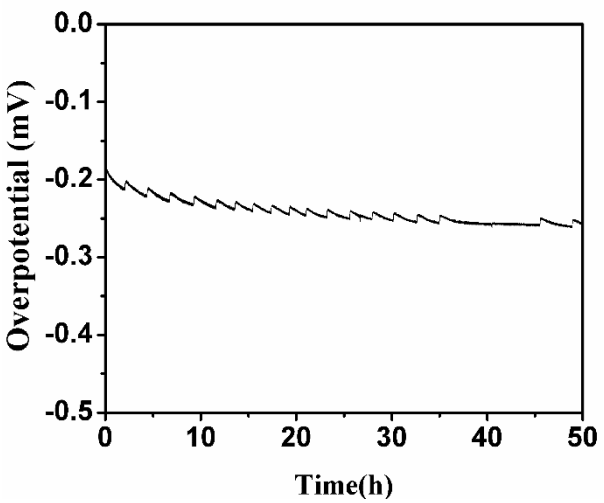

Figure 6. The time-dependent current overpotential curve of $Co_{8.5}$-$Ni_{1.5}$-B-P nanocomposites catalysts.

4. CONCLUSIONS

In summary, a series of amorphous Co_{10-x}-Ni_x-B-P nanocomposite catalysts were successfully synthesized via a simple chemical reduction and phosphorization. After the phosphorization, the $Co_{8.5}$-$Ni_{1.5}$-B-P nanocomposite catalysts exhibited the highest electrocatalytic HER activity in alkaline solution and required overpotentials of only 145 mV and 162 mV at current densities of 10 mA cm^{-2} and 20 mA cm^{-2}. The durability of the $Co_{8.5}$-$Ni_{1.5}$-B-P catalyst showed no obvious degradation after 50 h at a current density of 10 mA cm^{-2}.

ACKNOWLEDGEMENTS
This work was supported by the National Natural Science Foundations of China (No. 21473128).

References

1. F. Wang, T. A. Shifa, X. Zhan, Y. Huang, K. Liu, Z. C. C. Jiang and J. He, *Nanoscale*, 7(2015)19764.
2. J. Zhang, X. Li, Y. Liu, Z. Zeng, X. Cheng, Y. Wang, W. Tu and M. Pan, *Nanoscale*, 10(2018)11997.
3. P. Wang, Z. Pu, Y. Li, L. Wu, Z. Tu, M. Jiang, Z. Kou, I. S. Amiinu and S. Mu**,** *ACS Appl. Mater. Inter*., 9(2017)26001.
4. K. Xu, P. Chen, X. Li, Y. Tong, H. Ding, X. Wu, W. Chu, Z. Peng, C. Wu and Y. Xie, *Am. Chem. Soc*., 137(2015)4119.

5. Y. Li, H. Wang, L. Xie, Y. Liang, G. Hong and H. Dai, *Am. Chem. Soc*., 133(2011)7296.
6. S. Bai, C. Wang, M. Deng, M. Gong, Y. Bai, J. Jiang and Y. Xiong, Angew. Chem. Int. Ed., 53(2015)12120.
7. M. Cabán-Acevedo, M. L. Stone, J. R. Schmidt, J. G. Thomas, Q. Ding, H. C. Chang, M. L. Tsai, J. H. He and S. Jin, Nat. Mater., 14(2015)1245.
8. M. S. Faber, and S. Jin, *Energy. Environ. Sci*., 7(2014)3519.
9. X. Guo, P. Zhang, X. Liu, N. Zhang, M. Jiang, Q. Kang and D. Shen, *Int. J. Electrochem. Sci*., 12(2017)2852.
10. Y. Hong, W. Zhang, Z. Wen and S. Ci, *Int. J. Electrochem. Sci*., 11(2016)8801.
11. J. T. Ren, L. Chen, C. C. Weng and Z. Y. Yuan, *Mater*.*Chem*.Front., 10(2018)1039.
12. R. Zhang, C. Zhang and C. Wei, *J. Mater. Chem. A*.,4(2016)1039.
13. Z. Chen, Q. Kang, G. Cao, X. Ning, H. Dai and W. Ping, *Int. J. Hydrogen Energy*, 43(2018)6076.
14. J. Masa, I. Sinev, H. Mistry, E. Ventosa, M. D. L. Mata, J. Arbiol, M. Martin, R. C. Beatriz and S. Wolfgang, *Adv. Energy Mater*., 7(2017)1700381.
15. G. Liu, D. He, R. Yao, Y. Zhao, and J. Li, *Nano Res*., 11(2018)1664
16. M. Zhuang, X. Ou, Y. Dou, L. Zhang, Q. Zhang and R. Wu, *Nano Lett*., 16(2016)4691.
17. E. J. Popczun, J. R. Mckone, C. G. Read, A. J. Biacchi and R. E. Schaak, *J Am Chem Soc*., 135(2013)9267.
18. C. Du, L. Yang, F. Yang, G. Cheng and W. Luo, *ACS. Catal.*, 7(2017)4131.
19. H. Li, Y. Wu, Y. Wan, J. Zhang, W. Dai and M. Qiao, *Catal. Today*, 93(2004)493.
20. Y. Li, H. Zhang, M. Jiang, Y. Kuang, X. Sun and X. Duan, *Nano Res*., 9(2016)2251.
21. Y. Bai, H. Zhang, L. Liu, H. Xu and Y. Wang, *Chem. - Eur. J.*, 22(2016)1021.
22. R. L. Wells, M. F. Self, A. T. Mcphail, S. R. Aubuchon, R. C. Woudenberg and J. P. Jasinski, *Organometallics*, 12(1993)2832.
23. X. Ren, C. H. Jiang, X. M. Huang and D. D. Li, *Physica. E*., 41(2009)349.
24. K. L. Stamm, J. C. Garno, G. Y Liu and S. L. Brock, *J Am Chem Soc*., 125(2003)4038.
25. X. Wang, P. Clark, S. T. Oyama, *J Catal*., 208(2002)321.
26. Z. Pu, A. I. Saana, M. Wang, Y. Yang and S. Mu, *Nanoscale*, 8(2016)8500.
27. M. C. Biesinger, B. P. Payne, L. W. M. Lau, A. Gerson and R. S. C. Smart, *Surf. Interface Anal.*, 41(2009)324.
28. B. Zhang, C. Xiao, S. Xie, J. Liang, X. Chen and Y. Tang, *Chem mater*., 28(2016)6934.
29. J. Masa, P. Weide, D. Peeters, I. Sinev, W. Xia, Z. Sun, B. Christoph, M. Martin and S. Wolfgang, *Adv Energy Mater*., 6(2016)1502313.
30. H. Li, H. Li, W. L. Dai, W. Wang, Z. Fang and J. Deng, *Appl Surf Sci*., 152(1999)25.
31. L. L. Feng, G. T. Yu, Y. Y. Wu, G. D. Li, H. Li, Y. H. Sun, T. Asefa, W. Chen and X. X. Zou, *Am.Chem. Soc*., 137(2015)14023.
32. L. G. Feng, H. Vrubel, M. Bensimon and X. L Hu, *Phys. Chem. Chem. Phys*., 16(2014)5917.
33. M. Ledendecker, S. K. Calderon, C. Papp, H. P. Steinruck, M. Antonietti and M. Shalom, *Angew. Chem*., 127(2015)12538.
34. D. Ansovini, C. J. J. Lee , C. S. Chua, J. Ong and Y. F. Lim . *J Mater Chem A., 4*(2016)1587.
35. T. J, L. Q, A. M. Asiri and S. X. *J Am Chem Soc.,* 136 (2014)7587.
36. A. Irshad and, N. Munichandraiah . *ACS Appl Mater Inter.*, 19746 (2017)19755.
37. Y. Feng, X Y Yu and U Paik. *Chem Commun.*, 52 (2016)1633.
38. Y. Shi and B. Zhang, *Chem Soc Rev*., 45(2016)1781.